HHS Public Access

Author manuscript

Cell Rep. Author manuscript; available in PMC 2016 April 15.

Published in final edited form as:

Cell Rep. 2016 April 12; 15(2): 372–385. doi:10.1016/j.celrep.2016.03.022.

Two-Step Reactivation of Dormant Cones in Retinitis Pigmentosa

Wei Wang[1,7], **Sang Joon Lee**[1,4,7], **Patrick A. Scott**[1], **Xiaoqin Lu**[1], **Douglas Emery**[1], **Yongqin Liu**[1,3], **Toshihiko Ezashi**[5], **Michael R. Roberts**[5], **Jason W. Ross**[6], **Henry J. Kaplan**[1], and **Douglas C. Dean**[1,2,3]

[1]Department of Ophthalmology & Visual Sciences, University of Louisville Health Sciences Center, Louisville, KY 40202

[2]Molecular Targets Program, James Graham Brown Cancer Center, University of Louisville Health Sciences Center, Louisville, KY 40202

[3]Birth Defects Center, University of Louisville Health Sciences Center, Louisville, KY 40202

[4]Department of Ophthalmology, College of Medicine, Kosin University, South Korea

[5]Division of Animal Sciences, University of Missouri, Columbia, MO

[6]Department of Animal Scineces, Iowa State University, Ames, IA

Abstract

Most Retinitis Pigmentosa (RP) mutations arise in rod photoreceptor genes, leading to diminished peripheral and nightime vision. Using a pig model of autosomal-dominant RP, we show glucose becomes sequestered in the retinal pigment epithelium (RPE), and thus is not transported to photoreceptors. The resulting starvation for glucose metabolites impairs synthesis of cone visual pigment -rich outer segments (OS), and then their mitochondrial-rich inner segments dissociate. Loss of these functional structures diminishes cone-dependent high-resolution central vision, which is utilized for most daily tasks. By transplanting wild-type rods, to restore glucose transport, or directly replacing glucose in the subretinal space, to bypass its retention in the RPE, we can regenerate cone functional structures, reactivating the dormant cells. Beyond providing metabolic building blocks for cone functional structures, we show glucose induces thioredoxin-interacting protein (Txnip) to regulate Akt signaling, thereby shunting metabolites toward aerobic glucose metabolism and regenerating cone OS synthesis.

Address correspondence to: Douglas C. Dean, University of Louisville Health Sciences Center, 301 E. Muhammad Ali Blvd., Louisville, KY 40202, Phone: 502-852-4882, douglas.dean@louisville.edu.

7These two authors had an equal contribution

AUTHOR CONTRIBUTIONS

W.W., S.J.L., D.D. and H.K. conceived and designed experiments. W.W. and S.J.L performed cell transplants and glucose injection, and most immunohistochemistry. X.L. and Y.L. performed immunohistochemistry, situ hybridizations and PCR. D.E. performed and analyzed ERGs. M.R.R. and T.E. generated and characterized pig iPS cells. P.S. did the transmission EMs. J.R. breed P23H pigs. W.W., S.J.L., H.J.K. and D.D. analyzed data and wrote the paper.

Introduction

Mutations in rod-specific genes in Retinitis Pigmentosa (RP) lead to diminished peripheral vision and dark adaptation (i.e., night-time vision). Viral gene replacement therapy is showing promise in complementing recessive and X-linked mutations (Bainbridge et al. 2015; Beltran et al. 2015; Jacobson et al. 2015). However, dominant-acting mutations are more complex to treat with gene therapy (Boyce et al. 2013). Many dominant mutations arise in the rod opsin, *RHO* (Morrow et al. 1998; Van Soest et al. 1999). Mutant RHO becomes trapped in the endoplasmic reticulum (ER), and the rods eventually undergo apoptosis (Roof et al. 1994; Price et al. 2011; Sakami et al. 2011). With rod degeneration, cone photoreceptors begin to lose function. Cones concentrated in the macula are responsible for high-resolution daylight vision utilized for reading, facial recognition and other daily tasks, and their loss of function is the most debilitating aspect of RP. This diminished cone function is highlighted by loss of functional structures including visual pigment-rich outer segments (OS), and mitochondrial-rich inner segments (IS) (Cai et al. 2014; Litts et al. 2015; Wong and Kwok 2016). Despite the loss of functional structures, there is long-term persistence of macular cone cell bodies consisting of little more than a nucleus in RP patients, which has been referred to as dormancy (Lin et al. 2009; Busskamp et al. 2010; Busskamp et al. 2012; Sahel et al. 2013; Wong and Kwok 2016). Although neuroprotective agents show promise in delaying onset of cone dormancy in RP animal models, they do not cause reassembly of cone IS or reactivation of OS synthesis, and thus, restoration of electrophysiologic function in dormant cones (Sahel et al. 2013). However, the persistence of dormant cones in RP patients and animal models raises the possibility that endogenous pathways for IS assembly and OS synthesis might be subject to reactivation in these cells.

Photoreceptors are among the most metabolically active cells, and like other neurons they depend upon glucose (Hurley et al. 2015), which appears to be used primarily in normal cones for OS synthesis (Ait-Ali et al. 2015). Circulating glucose from the choriod is transported to the retinal pigment epithelium (RPE) and then into the subretinal space for uptake by a Glut1 complex on photoreceptor IS (Gospe et al. 2010; Ait-Ali et al. 2015). Recent studies suggest the thioredoxin family member rod-derived cone vaibility factor (RdCVF) can promote glucose uptake into cones in cell culture (Ait-Ali et al. 2015), and its overexpression in the subretinal space is neuroprotective and can delay transition to cone dormancy in rodent RP models (Bryne et al. 2015; Sahel et al. 2013). But, it is unclear whether these neuroprotective effects in vivo are linked to the promotion of glucose uptake seen in cell culture.

We have developed a pig model of autosomal-dominant RP where cones are concentrated in a visual streak and transition to dormancy with rod degeneration (Hendrickson and Hicks 2002; Ross et al. 2012; Scott et al. 2014). Our results provide evidence glucose becomes sequestered in the RPE and is not transported to photoreceptors in the RP retina. Transplant of WT rod precursors restored glucose transport to photoreceptors, reestablishing cone OS synthesis and electrophysiologic function. Likewise, direct injection of glucose into the subretinal space, to bypass its retention in the RPE, rapidly restored cone OS synthesis and electrophysiologic function in the absence of rods. Beyond simply providing metabolites for

synthesis of OS, we present evidence glucose directs its own metabolic pathway in cones. We show constitutive Akt activation, which is a hallmark of cancer cells that drives anaerobic metabolism (i.e., the Warburg effect) (Chen et al. 2008; Hui et al. 2008; Cernigila et al. 2015; Warburg 1956), also highlights dormant cones. Glucose induction of thioredoxin-interacting protein (Txnip), the most highly glucose-inducible gene identified to date, regulates Akt activity to divert cells toward aerobic glucose metabolism and fatty acid synthesis (Chen et al. 2008; Hui et al. 2008; Cerniglia et al. 2015). We provide evidence in cones that glucose induction of Txnip is key in regulating Akt activity and directing glucose metabolism toward OS synthesis.

Results

A pig model of autosomal dominant RP with progressive loss of cone function

The most common autosomal-dominant mutation in North America responsible for RP is a P23H mutation in RHO. As in RP patients, P23H RHO pigs initially form rod OS (Figs. 1A; S1). We then followed changes in outer retinal histology in the region of the cone-rich visual streak. While WT rod OS rapidly extend after birth, P23H RHO begins to be trapped in rod IS at postnatal day (P)2, and by P3 WT RHO was trapped in the ER of IS along with P23H RHO, correlating with loss of rod OS in the mutant pigs (Figs. 1B–E; S1) (Saliba et al. 2002; Tam et al. 2010). Then at P7, in many rods the IS ER collapsed into the cell body and both P23H and WT RHO became confined to a perinuclear ER-like structure (Fig. 1F–F″). By P30, RHO expression was lost, and the ONL was reduced to approximately two rows (Figs. 1G). In the pig, the outer two rows of the ONL are comprised only of cones (Fig. 2A; Wang et al. 2014). Although cone OS were similar in P23H and WT litter mates prior to birth (Fig. S1), following trapping of RHO in the ER, and in turn loss of rod OS initiating at P2 in the P23H retina (Figs. 1B–D; S1), cone OS truncation and loss was already evident in many cones at P3 (Figs. 1D; S1). By, P14 cone OS loss progressed and most cone OS were lost by P30 (Fig. 2B–F; S1). At P30, cones comprised most of the ONL, and any persisting rod cell bodies lacked RHO expression and showed compacted, dense nuclei (Fig. 1G and 2F). By, P60, all rod cell bodies were lost and the ONL was comprised only of cones with IS but no OS (Fig. 2G). At P120, the cone IS cilium is lost (Fig. 2H). By P130, the ER marker calnexin migrated from its normal position in the IS to a perinuclear location in the cell body, and likewise, mitochondria normally concentrated in the IS ellipsoid, also migrated to a perinuclear postion (Fig. 2I–K′), reflecting disassembly of these functional components of the IS. But, despite this loss of both OS and IS structures, cone cell bodies persisted for at least 4 years in P23H retinas. We concluded transition to cone dormancy is a two-step process highlighted first by immediate initiation of loss in cone OS synthesis with rod OS loss, which preceded any decrease in rod cell number. Following a protracted four month period, the ER and mitochondria in cone IS migrated into the cell body (which we refer to hereafter as cone IS disassembly), reflecting end-stage cone dormancy. Thus, the P23H pig represents a large animal model of autosomal-dominant RP where cones are concentrated into a visual streak, and their transition to dormancy in this region initiates with onset of rod degeneration following birth.

Transplanted WT rod precursors preserve endogenous cone OS and electrophysiologic function

We asked if transplantation of WT rod precursors might preserve endogenous cone OS and electrophysiology in P23H pigs. For these studies, we initially utilized rod precursors from embryonic day (E)65 GFP^+ pigs (gestation is ~113 days). Cone precursors differentiate before rod precursors in the pig, and we have previously demonstrated that by E65 remaining photoreceptor precursors in the pig retina are almost solely committed to the rod lineage, and these E65 cells formed RHO^+ OS following transplant into the subretinal space (Wang et al. 2014). 5×10^5 cells were injected in 50 μl into the subretinal space beneath the visual streak of one eye of P23H pigs at P14, as we previously described in detail, and pigs were assessed for cone electrophysiologic function using electroretinography (ERG) under daylight (photopic) conditions, and then for retinal histology and immunostaining at P60 (Wang et al. 2011; Zhou et al. 2011; Wang et al. 2014) (Methods). Contralateral eyes were used as a sham transplant control with injections of diluent alone. GFP was used to follow the transplanted cells. We found that these GFP^+ transplanted cells either integrated into the ONL or formed a monolayer apposed to the ONL (Fig. 3A–B′; S2). In either case, the transplanted cells formed long RHO^+ OS extending to the RPE (Fig. 3A–B′; S2). Transplant sites were ~500 μm in diameter, and serial 20 μm sections were analyzed in four directional vectors throughout each site to evaluate the number of GFP^+ cells with RHO^+ OS, as we have described (Wang et al. 2014) (Methods). We found an average of 5433±733 GFP^+ cells with RHO^+ OS per injection site (n=5). By contrast, only 421±408 GFP^+/Cone $Opsin^+$ cells were seen, again emphasizing that most of the precursors persisting at E65 are committed to the rod lineage, as noted above. Additionally, we found <100 GFP^+ cells that did not express RHO or cone opsin, indicating that most cells expressed RHO following transplant. Next, we attempted to transplant more cells, but with 1×10^6 cells we found many of the cells formed aggregates in the subretinal space (Fig. S2). Although GFP^+ cells within these aggregrates expressed RHO, the cells failed to extend OS toward the RPE (Fig. S2).

We found that monolayers of transplanted GFP^+ cells extending RHO^+ OS, resulting from transplant of 5×10^5 cells, maintained endogenous (GFP^-) cone OS out to a distance of approximately 1000 μm from the transplant site (Fig. 3C–E; S2). No effect on cone OS was seen with the sham transplant (Fig. 3F), nor was an effect evident when 1×10^6 cells were transplanted and aggregrates formed in the subretinal space (Fig. S2). Consistentent with maintenance of endogenous cone OS by monolayers of transplanted cells, cone electrophysiology was increased in regions surrounding these transplant sites using photopic multifocal ERG (mfERG) (Figs. 3G; S2). However, we did not observe a reproducible effect of transplanted rods on the photopic full field ERG (ffERG), which measures the global electrophysiologic response (i.e., the entire retina.

We have described generation and efficient differentiation of iPS cells derived from GFP^+ pig skin fibroblasts into rod precursors in culture (Zhou et al. 2011). We found that 34±6% of the differentiating iPS cells in culture expressed the rod precursor marker NRL and 27±7% expressed RCVRN, but only 8±3 % of the cells in culture expressed the terminal rod differentiation marker RHO (Zhou et al. 2011). Such Nrl^+, Rho^- rod precursors in the mouse were found to most efficiently integrate into the retina and go on to express Rho^+ OS

following subretinal transplant, and we previously found that these differentiated pig iPS cells formed RHO^+ OS following subretinal transplant. Therefore, we asked whether injection of GFP^+ differentiated iPS cells would mimic the E65 rod precursors and perserve cone OS and mfERG in P23H pigs. As with E65 rod precursors, endogenous cone OS were preserved out to approximately 1000 μm from the iPS cell injection site, whereas the sham transplant in the contralateral eye had no similar effect (Fig. S3). Consistent with preservation of cone OS, the photopic mfERG was maintained only in regions surrounding injection sites (Fig. S3).

Together, these findings provide evidence that transplantation of WT rod precursors into the visual streak at P14 can delay transition of cones to dormancy in regions surrounding transplant sites in a pig model of dominant RP. This effect was not simply linked to the number of transplanted cells, but instead to the ability of the cells to form a monolayer and extend RHO^+ OS toward the RPE.

Transplanted rod precursors reactivate end-stage dormant cones, restoring IS assembly, OS synthesis and electrophysiologic function

Next, we transplanted 5×10^5 E65 GFP^+ rod precursors into the subretinal space of P23H pigs at 18 months of age, where dormant cones lacking both IS and OS were the only cells remaining in the ONL of the visual streak. Again, monolayers of transplanted GFP^+/RHO^+ cells with long OS were evident at injection sites (Fig. 4A–A′). Notably, $calnexin^+$ IS and cone $opsin^+$ OS were restored in endogenous cones in a region extending out to approximately 1200 μm from transplant sites (Figs. 4B–H; S3; S4). Although cone OS diminished at 1200 μm, with cone opsin becoming confined to $calnexin^+$ IS at this location, $calnexin^+$ IS persisted out to approximately 1600 μm (Fig. 4B–H), demonstrating that reassembly of IS can occur in the absence of, and thus, be dissociated from reactivation of OS synthesis. Photopic mfERGs surrounding transplant sites showed an increase, correlating with endogenous cone OS restoration (Figs. 4I; S3). These results provide evidence that transplant of rod precursors into a rodless retina locally restores cone IS and OS, and in turn cone electrophysiologic function, thus reversing end-stage dormancy. When rod precursors were transplanted into two sites within the visual streak in these experiments, we observed an increase in the amplitude of the photopic b-wave and flicker response in the ffERG (Figs. 4J and K). These results provide evidence that increasing the number of cell transplant sites produces an additive effect, leading to an observable increase in cone electrophysiology in the full retina.

It is of note that a background photopic ffERG signal persisted in the P23H pigs, despite the loss of cone OS and IS in the visual streak (Fig. 4J–K). Cone density in the domestic pig is 39,000 cones/mm^2 in the streak vs 8,500 cones/mm^2 in the peripheral retina (Chandler et al. 1999). Thus, there are a substantial number of cones outside the streak in the peripheral retina. Likewise, although cones are concentrated centrally in the human macula, there is also a high concentration of cones in a 1 mm band at the peripheral edge of the retina, where cone density rises 3-fold and rod density diminishes 10-fold (Williams 1991). We then examined the peripheral retina in P23H pigs. Although rods are diminished by P30 in the visual streak (Fig. 1G), rod degeneration was delayed in the peripheral retina, where rod OS

were still evident at P60 and cone OS and IS persisted (Fig. S4). Rods were eventually lost by P130 in the peripheral retina, but cone IS and OS were maintained in this region as P23H pigs aged (Fig. S4). It is unclear why cone functional structures are maintained in the absence of rods in the peripheral retina, but it might be related to lower cone density in this region, and thus, less competition for available glucose (see below). It is not possible to measure mfERG in the peripheral retina; however, we suggest that persistence of cones functional structures in the peripheral retina is responsible for the background photopic ffERG that persists after cones in the visual streak become dormant. Indeed, the mfERG in the visual streak was low and near the threshold of detection (Fig. 4I), further suggesting that the persisting ffERG signal is not arising from the streak. Nevertheless, despite the background ERG signal arising from peripheral cones, two transplant sites within the streak were able to increase the ffERG.

Rod loss appears to limit cone access to glucose

Our results above demonstrated that transplant of rod precusors restores cone IS assembly and OS synthesis, thereby reversing cone dormancy in the visual streak of the P23H retina. These findings demonstrate rods are doing more than simply delaying cone transition to dormancy. We then wondered if these transplanted rods might be affecting access of dormant cones to glucose. To begin testing this model, we initially examined expression of Txnip, the most highly glucose-inducible gene identified to date, and which regulates the balance between anaerobic vs. aerobic metabolism that is classically altered in diabetes and cancer (Xu et al. 2013; Yoshioka et al. 2012; DeBalsi et al. 2014) (see Fig. 7A below). We found that Txnip was induced at birth in WT pigs in the ellipsoid of cone IS, where mitochondria are concentrated, and persisted in the adult (Fig. 4L–O; results not shown). Txnip was not detected in rods or the RPE. And, Txnip mRNA was low in RPE and Muller cells in primary culture (Fig. 4P). In contrast to WT pigs, rod OS are lost following birth in the P23H retina as the light-induced conformation change in P23H RHO causes it to become trapped in the ER (Sailba et al. 2002) (Figs. 1B–D; S1), and Txnip was not evident in cones of P23H pigs at any age (Fig. 4O; results not shown). Additionally, Txnip mRNA was low in the P23H retina compared to WT (Fig. 4P). These results examining the glucose sensor Txnip provided initial evidence that cone access to glucose in vivo is somehow dependent upon WT rods.

Glucose becomes sequestered in the RPE and is not transported to photoreceptors in the P23H retina

Next, we followed glucose transport from the circulation into photoreceptors in vivo utilizing fluorescently labeled 2-deoxy-glucose (Fig. 4Q–T′). For these experiments, we turned to the P23H Rho knock in mouse where retinal tissue can be quickly frozen and rapidly cut and analyzed before glucose diffusion occurs. Two sources supply blood to the mammalian retina. Choroidal vessels maintain the outer retina (photoreceptors), whereas the central retinal artery from the optic nerve head supplies blood to the inner retina. As opposed to the direct inner retinal circulation, glucose from the choroid is transported first to the RPE and then from the RPE into the subretinal space, where it is taken up into photoreceptors via Glut1 receptor complexes on IS (Ait Ali et al. 2015). Mice where the P23H Rho mutation was knocked into one allele and WT liter mate controls (Sakami et al. 2011) were injected

with 150 ul of 10 uM 2-deoxy-glucose in the tail vein at P35 (n=5). At this time, the ONL was maintained, rods were beginning to show shortening of their OS and cones appeared histologically normal (Fig. 4Q and S). Previous studies in mice showed peak uptake of fluoresecently labled glucose from the circulation into tissues between 45 min to 1 hr after injection, with subsequent loss of tissue labeling after this time point (Rajaram et al. 2013; Frees et al. 2014). Therefore, we followed uptake into the eye at 15 min, 1 hr and 2 hr after injection, as described (Rajaram et al. 2013; Frees et al. 2014). We did not observe uptake at 15 min., and by 2 hr glucose fluorescence in the eye had already diminished (results not shown). After 1 hr, labeling of the inner retina appeared similar in the WT and mutant mice; however, there was a dramatic difference in labeling of the outer retina (Fig. 4R–R′ and T–T′). Both rod and cone IS were highly labeled in the WT retina, but they were not labeled in the P23H retina. By contrast, the RPE was highly labeled in the P23H retina, whereas little labeling of RPE was evident in the WT retina. We conclude delivery of glucose to the inner retina is not affected in the P23H retina, but with onset of rod OS shortening, glucose accumulates in the RPE and is no longer transported to either rod or cone photoreceptors in the P23H retina.

Transplanted rod precursors restore cone access to glucose

We then wondered if transplanted rods were restoring access of dormant cones to glucose. Indeed, we found that Txnip was induced in endogenous cone IS following rod precursor transplants into 18 month-old P23H pigs (Figs. 4F–H; S3). This Txnip induction surrounded the injection site and correlated with regeneration of endogenous IS and Opsin^{+} OS. Likewise, we also observed Txnip induction in endogenous cone IS in a similar pattern when rod precursors were transplanted into the subretinal space at P14. Based on this induction of Txnip, we concluded that transplantation of rod precursors was likely restoring cone access to glucose in a radius corresponding to approximately 1200 μm around the transplant site, and this glucose access is closely linked to restoration of endogenous cone OS synthesis.

Subretinal glucose replacement in a rodless retina reactivates cone OS synthesis and induces Txnip, the miR 96/182/183 cluster and fatty acid synthesis enzymes

Taken together, the above results provided evidence glucose becomes sequestered in the RPE and is not delivered to photoreceptors in the P23H retina. Transplant of WT rod precursors appeared to restore glucose transport to cones, reactivating OS synthesis and electrophysiologic function in the dormant cells. We then wondered if injection of glucose into the subretinal space in the visual streak would bypass its sequesteration in the RPE and reverse cone dormancy. Glucose has been delivered subretinally at a concentration of 280 mM with no evident effect on retinal histology or ERG (Penha et al. 2007). We anticipated that achieving a concentration of 1–3 mM glucose in the subretinal space would be sufficient for cone function (Penha et al. 2007), and this would occur in a gradient as concentrated glucose diffused from the injection site. Therefore, we injected glucose at a concentration of 280 mM in a 50 μl volume into the subretinal region of the visual streak in P23H pigs at P45, when rods are lost and cones retain IS but no OS. Media was injected as a control in the contralateral eye. After three days, we compared retinal histology and immunostaining in the glucose injected and sham control eyes. We found that Opsin^{+} cone OS were restored in a

~1500 μm radius from the site of glucose injection, and we observed glucose induction of Txnip paralleling this cone OS restoration (Fig. 5A–B).

Our results above implied that glucose in cones is being utilized for OS synthesis. Long chain fatty acids are essential components of OS, and key ezymes in the fatty acid synthesis pathway are known to be regulated by glucose. Acetyl CoA carboxylase (ACC) catalyzes the carboxylation of acetyl-CoA to malonyl-CoA. Then, fatty acid synthase (FAS) catalyzes formation of fatty acids from acetyl-CoA, malonly-CoA and NADPH. These fatty acid synthesis pathway enzymes are induced by glucose via carbohydrate response element binding protein (ChREBP), a glucose responsive transcription factor, and a second transcription factor, sterol response element binding protein (SREBP), whose expression is also induced by glucose/insulin (Lumayag et al. 2013; Jeon et al. 2013; Xu et al. 2013; Busskamp et al. 2014). SREBP entry into the nucleus and its turnover has been shown to be regulated by Fbxw7 and Insig2 in the liver, which limits its activity (Fig. S5) (Jeon et al. 2013). Within a positive feedback loop, SREBP induces the miRNA cluster of miR96/182/183, which in turn targets Fbxw7 and Insig2 to fully activate SREBP. These miRNAs are transcribed as a single transcript, which is then processed to the individual miRNAs. Importantly, knockdown or mutation of this cluster leads to loss of cone OS and electrophysiology (Busskamp et al. 2014). Conversely, forced expression was sufficient to trigger cone OS synthesis in embryonic stem cells undergoing photoreceptor differentiation in culture (Busskamp et al. 2014). However, it has not been investigated wherther regulation of SREBP by miR96/182/183 is the reason the cluster is critical for cone OS synthesis and function.

We followed miR183 expression by in situ hybridization, as representative of the miR 96/182/183 cluster transcript, and FAS and ACC by immunostaining (Fig. 5A–B). We found miR183 was absent in cones of P23H pigs at P45, but was rapidly induced by glucose in these cells within three days after injection. This glucose induction of miR183 paralleled that of Txnip and cone OS regeneration extending from the site of glucose injection (Fig. 5B). We found that ACC and FAS were also induced in endogenous cones in P23H pigs adjacent to transplanted rods, as well as when glucose was injected into the subretinal space (Fig. 5A–B; results not shown).

We conclude retention of glucose by the RPE in the P23H retina causes loss of cone OS synthesis, leading to dormancy. Glucose not only provides metabolites for cone OS formation, it also induces the fatty acid synthesis pathway, which we suggest directs these metabolites toward OS synthesis in the cells.

Glucose replacement restores dormant cone electrophysiology in P23H pigs to a WT level

Consistent with restoration of cone OS synthesis, we found that glucose injection into the subretinal space in the region of the streak at P45 in the P23H retina increased the photopic mfERG in the region of the injection, even though rods are absent in this region (Figs. 5C; 1G and S1). Injection of control media into the contralateral eye did not affect the mfERG. As with rod precursor transplants above, subretinal injection of glucose into two sites increased the photopic ffERG (Fig. 5D–E). Notably, this ffERG response was more robust than that seen following rod precursor transplant (Fig. 4J–K), leading to rapid restoration of

photopic the ffERG to a level similar to that seen in WT liter mates (Fig. 5D–E). Notably, this reactivation of dormant cone OS synthesis and electrophysiology by glucose in the absence of rods has not been seen with any neuroprotective agent to date.

IS disasssembly is a barier to glucose-induced reactivation of OS synthesis in end-stage dormant cones

The above results demonstrated that glucose replacement in the subretial space was sufficient to rapidly reactivate cone OS synthesis and electrophysiologic function in the P23H retina, but these studies were done at P45, prior to loss of cone IS. Because mitochondrial-dependent acetyl-CoA generation from glucose is required for fatty acid synthesis, we wondered whether glucose replacement alone would be sufficient for restoration of OS synthesis after mitochondrial-rich IS were lost. Thus, we repeated the glucose subretinal injection experiments in older P23H pigs at P130, where dormant cones in the streak had progressed to lose their IS (Fig. 2H–K′). In these older pigs, glucose replacement failed to restore cone IS, cone OS or electrophysiology (results not shown). We concluded that IS assembly is a prerequisite for glucose-induced restoration of cone OS synthesis, and thus, glucose replacement to reactivate cone OS synthesis is only effective before dormant cones progress to the end-stage point of IS disassembly. Nevertheless, dormant cones in the streak lose OS synthesis initially and in P23H pigs there is a four-month delay before IS disassembly occurs. Thus, there is a substantial window for reactivation of OS synthesis in dormant cones with glucose replacement before end-stage disassembly of IS occurs.

Txnip is required for cone OS synthesis and function

Beyond simply providing metabolites for cone OS synthesis, glucose induces gene transcription, and our results above show glucose induces the fatty acid synthesis pathway in cones, which might be critical to direct its metabolic pathway in these cells. We then initiated studies to further examine how glucose might be regulating its own metabolism in cones. Pyruvate dehydrogenase (PDH) is the “gatekeeper” for aerobic glycolysis, and it catalyzes acetyl CoA production from glucose-derived pyruvate for fatty acid synthesis. Notably, acetyl CoA is also the entry point into the TCA cycle, where resulting isocitrate and malate act as precursors for most of the NADPH used in the visual cycle (Adler et al. 2014). Consistent with an important role for PDH in cone function, patients with PDH deficiency not only display neurologic abnormalities, they also progress to central vision loss (Brown et al. 1994). And, knockdown of PDH in Zebrafish led to loss of cone function (Taylor et al. 2004). The PDHε subunit is inhibited by Akt-dependent phosphorylation to block mitochondrial metabolism and drive glucose-derived pyruvate into anaerobic metabolism for ATP production in cancer (Chen et al. 2008; Hui et al. 2008; Cernigila et al. 2015). Txnip regulates Pten to control downstream Akt activity, and it is thus required to prevent inhibitory PDH phosphorylation, thereby promoting aerobic mitochondrial-based conversion of glucose-derived pyruvate into acetyl CoA for production of both fatty acids and NADPH (Yoshioka et al. 2013; DeBalsi et al. 2014) (see Fig. 7A below).

We hypothesized that the failure to induce Txnip in cones in the P23H retina would lead to constitutive Akt activation and a block in cone OS synthesis. To begin testing this

hypothesis, we compared Akt phosphorylation in WT retinas, where Txnip is expressed in cones, and P23H retinas where Txnip is not expressed. We found phosphorylated Akt (P-Akt) accumulated in P23H cones, where it was concentrated in IS (Fig. S5). Next, we examinined P-Akt in P23H cones following glucose injection into the subretinal space. P-Akt decreased in cones in parallel with glucose induction of Txnip and restoration of OS synthesis (Figs. 5A–B; S5). These results demonstrate that constitutive Akt activation highlights dormant cones, and suggest that glucose induction of Txnip might be required for preventing constitutive Akt activation in cones to permit OS synthesis.

To directly test a role for Txnip in Akt activation and cone OS synthesis, we used AAV8 transduction of Txnip shRNAs in WT pigs (Fig. S6). In this virus, Txnip shRNA and GFP are expressed from an 1.8 kb fragment of the elongation factor 1a (EF1a) gene promoter. As with transplantation of rod precursors and glucose injection above, virus was injected subretinally in 30 μl, consisting of 2×10^{10} vector genomes, at single sites above the optic nerve beneath the visual streak in WT pigs at P40. We have already demonstrated only cones comprise the outer two rows of the ONL in pigs, with rods confined to the inner rows of the ONL (Fig. 2A; Wang et al. 2014). It is then of note that GFP expression was evident in both rod and cone photoreceptors (Fig. 6A), demonstrating efficient infection of photoreceptors. By contrast, we did not observe GFP expression in RPE, Muller cells or cells in the inner retina. Lack of GFP expression in the inner retina, following subretinal injection, might reflect failure of the virus to efficiently penetrate to the inner retina under these conditions. But, AAV8 has been shown previously to infect the RPE in pigs following subretinal injection (Mussolino et al. 2011). However, these studies were done with viruses where GFP was driven by either a CMV promoter or a beta-actin promoter with a CMV enhancer. Although, a smaller 300 bp fragment of the EF1a promoter (lacking cell type specificity) has been utilized to drive expression in multiple cell types, it is of note that EF1a, while expressed in the developing RPE, is downregulated in adult cells, and in zebrafish it is only re-induced in RPE following retinal damage (Zheng and Baum 2014; Burket et al. 2008). Thus, it is likely that failure to observe GFP expression in the RPE is due to lack of promoter activity in these cells as opposed to no infection. We also tested the AAV Txnip shRNA in cell culture. Primary cultures of neural retina cells from pigs at P14 showed efficient GFP expression following infection, whereas little GFP expression was evident following infection of primary cultures of either RPE or Muller cells (Fig. S6).

We assessed effects of the Txnip shRNA and control viruses on electrophysiology, retinal histology and immunostaining four weeks after injection into WT pigs at P40. The control virus did not affect retinal histology, Txnip expression, cone OS formation, rod OS formation, or electrophysiology (Figs. 6A–K; S6). However, infection with the Txnip shRNA AAV caused downregulation of Txnip mRNA in the neural retina in vivo, and in primary culture of neural retina from P14 pigs (Fig. 6J; S6). GFP^+ cones infected with AAV expressing Txnip shRNA showed loss of immunostaining for Txnip (Fig. 6F and K). Importantly, these GFP^+ cones showed loss of cone $opsin^+$ OS and they accumulated activated P-Akt, whereas adjacent uninfected cones maintained OS and did not show P-Akt accumulation (Fig. 6G–I and K). Consistent with loss of cone OS in the infected cones, there was a decrease in the photopic mfERG in the region of Txnip shRNA virus injection, and some of the eyes showed diminished photopic ffERG (Figs. 6L; S6). By contrast, in the

same experiments, AAV Txnip shRNA infected rods continued to display RHO^+ OS and normal histology, and the ERG in dim light (scotopic) to analyze rod electrophysiology was not affected (Figs. 6E and K; S6). This would be expected, as we did not detect Txnip expression in rods. We conclude that beyond providing metabolites for cone OS synthesis, glucose induces expression of genes and miRNAs that direct its metabolism in cones. Induction of Txnip in cones prevents constitutive Akt activation, thereby allowing glucose metabolites to be diverted to aerobic metabolism, and then induction of the fatty acid synthesis pathway directs these metabolites toward generation of cone OS.

Discussion

Glucose transport to the outer retina

The most debilitating aspect of RP is diminished cone-dependent high resolution central vision. Because most mutations in RP occur in rod-specific genes, this accompaning loss of cone function is puzzling. Recent studies in primary cultures of cones show that purified RdCVF added to the cultures can bind a Glut1 complex on cone IS and promote glucose uptake into the cells (Ait-Ali et al. 2015). Because RdCVF is expressed by rods, loss of its expression following rod degeneration might therefore restrict glucose uptake into cones. However, it is unclear whether the neuroprotective effect of RdCVF overexpression seen in vivo involves regulation of glucose uptake. Our studies of the dynamics of glucose transport in the WT vs. P23H retina provide direct evidence of the problem with glucose in the RP retina. We link onset of diminished mutant rod OS extension to retention of glucose in the RPE, thereby preventing its transport to both persistant mutant rods as well as cones. Indeed, directly blocking rod OS formation by mutating the OS protein rds/peripherin (Kedziersji et al. 1998) also classically leads to RP with cone dormancy, supporting such a role for rod OS loss in initiation of RP. Because glucose becomes sequestered in the RPE of the P23H knock in retina well before mutant rod cell death (e.g., although diminished rod OS extension was evident at P35, extensive rod cell death did not occur for another two months), the ensuring glucose starvation of the mutant rods may contribute to their subsequent degradation. RdCVF does not affect glucose uptake into rods (Ait Ali et al. 2015), thus this failure of rods to take up glucose in the P23H retina is not due to a change in expression of RdCVF. In their model, overexpression of RdCVF in the subretinal space would be expected to drive uptake of diminishing levels of glucose in the subretinal space into cones as glucose becomes sequestered in the RPE, thereby delaying transition to cone dormancy. But, once glucose is sequestered in the RPE and cone OS syntheis is lost, RdCVF is not capable of reinitiating OS synthesis and reversing dormancy. Such reversal of dormancy requires either rod transplantation to re-establish glucose transport or glucose injection to bypass its retention in the RPE.

Cone survival and dormancy in RP

Glucose starvation of cones in the visual streak during RP leads to loss of functional structures. Yet, the cells survive in a dormant state with little more than a nuclues persisting. We show that cone dormancy is highlighted by constitutive Akt activation, implying loss of upstream Pten function. Beyond regulation of Akt activity to inhibit PDH activity and thereby drive anaerobic metabolism (responsible for loss of cone OS synthesis), the Pten

pathway is also a critical regulator of cell survival (Worby and Dixon 2014). Accordingly, diminished Pten activity has been shown to be key to cone cell survival in mouse models of RP (Venkatesh et al. 2015). The Pten phosphatase catalyses dephosphorylation of PIP3 to PIP2, which in turn negatively regulates two separate mTor kinase-dependent complexes in the cell (Worby and Dixon 2014; Masui et al. 2014). mTor complex 1 (mTorc1) promotes protein translation and is essential for maintaining translation, and thus, cell survival during hypoxia, anaerobic glycolysis, and glucose/nutrient starvation; in contrast, mTor complex 2 (mTorc2) catalyzes activating phosphorylation of Akt on serine 473 (the Akt activating phosphorylation we analyzed above), which is the key pathway cells utilize to metabolize glucose in response to insulin. This mTorc2/Akt pathway is frequently constitutively activated in cancer, driving cells into anaerobic glycolysis (Masui et al. 2014). Notably, these two mTor complexes are highlighted by a key difference--mTorc1 contains Raptor, whereas mTorC2 contains Rictor (Masui 2014). Importantly, it was shown that Raptor, and thus mTorc1, is the pathway through which Pten regulates cone survival in RP (Venkatesh et al. 2015). This would be consistent with the established mTorc1-dependent function of promoting survival in low glucose/nutrient conditions, noted above. It then appears that separable pathways downstream of Pten might branch to regulate cone survival and the Akt-dependent balance in aerobic vs. anaerobic metabolism.

Regulation of glucose metabolism in cones

The PDHε subunit is inhibited by Akt-dependent phosphorylation to block mitochondrial metabolism and drive glucose-derived pyruvate into anaerobic metabolism in cancer (Chen et al. 2008; Hui et al. 2008; Cernigila et al. 2015). Txnip is required to prevent this inhibitory phosphorylation, thereby promoting aerobic conversion of glucose-derived pyruvate into acetyl CoA for production of fatty acids and NADPH (Yoshioka et al. 2013; DeBalsi et al. 2014) (Fig. 7A). Although Txnip is induced by glucose, it feeds back to inhibit activity of Glut1, thereby limiting glucose uptake (Yoshioka te al. 2012; Xu et al., 2013; DeBalsi et al. 2014) (Fig. 7B). In this way Txnip tightly regulates the level of glucose in the cell. Further, palmitate, the product of ACC and FAS, feeds back to activate the master metabolic regulator, AMP kinase, which in turn inhibits Txnip (Anders et al. 2011). Thus, Txnip appears to serve as a hub to tightly regulate glucose metabolism to fatty acids.

Txnip is thioredoxin interacting protein, and is required for formation of an active NADPH-thioredoxin complex that reduces inhibitory disulfide bond formation in Pten (Hui et al. 2008). In the absence of Txnip in heart, skeletal muscle and fibroblasts, oxidized/inactive Pten accumulates leading to phosphorylation, and thus, constitutve activation of its downstream pathway component Akt. Then, as noted above, Akt in turn causes phosphorylation and inactivation of PDH, leading to diversion of glucose to anaerobic metabolism (Hui et al. 2008; Yoshioka te al. 2012). Our results provide evidence that glucose induction of Txnip is serving a similar function in regulating Akt activity in cones, thereby directing aerobic metabolism for OS synthesis.

Classically Txnip binds thioredoxin and inhibits its function in regulating ROS pathways and inflammatory complexes (DeBalsi et al. 2014). Yet, as noted above, it promotes thioredoxin-NADPH activity in maintaining active Pten and in turn preventing constitutive

Akt activation (Hui et al. 2008; Kwon et al. 2004). These seemingly contridictory functions can be rationalized by evidence that Txnip inhibits NADH production, which is an inhibitor of the thioredoxin-NADPH complex, and in these ways it is able to directly block some thioredoxin functions, while promoting NADPH production/activity and thus other thioredoxin functions. Indeed, such preservation of NADPH activity in cones might be important for the visual cycle as well.

Despite our finding that knockdown of Txnip in pig cones leads to loss of OS and electrophysiologic function, Txnip mutation in the mouse has not been linked to a loss in vision, and can prevent inflammation and vascular injury (El-Azab et al. 2014). It is of note that Txnip is a member of the α-arrestin family, and it is becoming clear that other family members also regulate metabolism and negatively regulate glucose uptake, like Txnip (Patwari and Lee 2012). So, species-specific patterns of expression of family members with overlapping functions might account for differences between pigs and mice.

Txnip in rods and cancer

As noted above, Txnip is a tumor suppressor whose mutation/repression in cancer is important in switching glucose metabolism from aerobic to anaerobic (e.g., the Warburg effect). But, why is Txnip not induced by glucose in cancer cells or rods, where glucose uptake is high? Accumulation of Hif1a in solid tumors is linked to the Warburg effect, where it acts at least in part by repressing Txnip (Marin-Hernandex et al. 2009; Geng et al. 2011). It has been demonstrated that HDAC activity is important for rod development and ongoing viability (Chen et al. 2007; Chen et al. 2009). HDAC4 function in rods has been examined specifically, and it requires Hif1a activity (Chen et al. 2009). Surprisingly, the activity of HDAC4 in rods was cytoplasmic (demonstrating its key function is not histone deacetylation at gene promoters in rods), where it promoted stabilization of Hif1a. Likewise, HDAC4 is also critical for accumulation of Hif1a in cancer (Geng et al. 2011). Because Hif1a represses Txnip, such activation of the HDAC4-Hif1a pathway might explain dominant Txnip repression in rods, as well as cancer cells, despite the presence of glucose. Indeed, such repression of Txnip would remove feedback to limit Glut1 activity (Fig. 7B), allowing deregulated glucose uptake. In cones, downregulation of Txnip, and thus release of Txnip inhibition of Glut1, might reflect an attempt to increase glucose uptake, as available glucose diminishes in RP.

Clinical implication of reversing cone dormancy

Because glucose transport from the RPE to photoreceptors appears diminished in RP, approaches aimed solely at neuroprotection or regulating metabolic pathways within cones will ultimately fail due to a lack of glucose metabolic building blocks for assembly of cone functional structures. We demonstrate two approaches for addressing this glucose problem. First, we show that WT rods can restore glucose transport to cones in the RP retina, thereby eliminating the problem, at least in the region of cell transplant. Multiple sites of cell transplantation appear to function additively to produce a detectable global retina electrophysiologic effect. Second, replacement of glucose in the subretinal space can bypass its retention in the RPE, and thereby rapidly and efficiently restore dormant cone OS syntheis and electrophysiology in the region of injection. Notably, injection of glucose at

two sites in the visual streak was sufficient to restore the full field retinal electrophysiologic respose to a WT level within 3 days in the absence of rods. Challenges remain in developing a therapeutic approach to provide long-term access of cones to glucose in the RP retina, and it is likely that the most successful approach will ultimately incorporate a combination of other therapies aimed at neuroprotection and metabolic pathways.

Methods

Embryonic retinal cell isolation and transplant, and glucose injection

All methods were approved by the University of Louisville Institutional Animal Care and Use Committee and adhered to the ARVO Statement for Use of Animals in Ophthalmic and Vision Research. GFP^+ precursor cells were isolated at E65 as described in detail previously (Zhou et al. 2011; Wang et al. 2014). 50 μl of cells or mediate containing 280 mM glucose were injected into two sites in the superior quadrant in the region of the visual streak, as described previously (Zhou et al. 2011; Wang et al. 2014). Following cell transplant or glucose injection, pigs were euthanized as retinas were analyzed form histology and immunostaing as described (Zhou et al. 2011; Wang et al. 2014). The number of GFP/RHO^+ cells forming monolayers and extending OS was counted in serial 20 μm sections spanning the entire transplant site as described (Zhou et al. 2011; Wang et al. 2014).

Photoreceptor differentiation of pig iPS cells

The swine iPSC photoreceptor differentiation protocol was described previously (Zhou et al. 2011). Cells expressing differentiation markers were counted and compared to the total number of cells found in each field, as determined by DAPI nuclear staining (Zhou et al. 2011). At least 2,000 cells were examined in each experiment. All sets of experiments were performed at least three times.

Immunostaining and transmission EM

Immunostaining of pig restinas was described previously (Zhou et al. 2011; Wang et al. 2014). The primary antibodies used were: mouse anti RHO (Millipore, 1:300), rabbit anti-NRL (a generous gift from Anand Swaroop, National Eye Institute, Bethesda, MD, 1:1000) (Wang et al. 2014) rabbit anti-calnexin (Thermo Scientific, 1:500), rabbit anti red-green opsin (OPN1LW/OPN1MW) (Millipore 1:500), chicken anti-JH492 and JH 455 anti-cone opsin (OPN1LW/OPN1MW) (gifts from Jeremy Nathans, Johns Hopkins 1:5000) (Wang et al. 2014), rabbit anti-ACACB (acetyl CoA carboxylate beta) (Novus 1:100), mouse anti-FAS (FASN) (Novus 1:100), mouse anti-NXNL2 (Genetex 1:100), Rabbit anti-NXNL2/TXNL6 (Proteintech, 1:200), Rabbit anti-Txnip (Abcam 1:100). Bound antibodies were visualized with either Alexa fluor 488- (Invitrogen 1:500) or Alexa Fluor 568- (Invitrogen, 1:500) conjugated secondary antibodies. We have described immunostaining for Akt phosphorylated on S473 previously (Liu et al. 2013 and 2014). Nuclei were counterstained with DAPI, and images were captured with a confocal microscope as described previously (Zhou et al. 2011; Wang et al. 2014). No immunostaining was evident in the absent of primary antibodies. Transmission EM was performed as described in detail previously (Scott et al. 2014).

miRNA in situ hybridization

For in situ hybridization to miR-183, retinas were fixed in 10% formalin solution immediately after removal, and then paraffin-embedded and sectioned at 10 μm. LNA-modified, double-DIG labeled DNA probes for miR-183 (5′-TATGGCACTGGTAGAATTCACTG) and scrambled control (5′-GTGTAACACGTCTATACGCCCA) were purchased from Exiqon (Denmark) and in situ hybridization was performed as we have decribed previously (Li et al. 2014), with the following modifications.

ERG recordings

Our detailed ERG protocols have been previously published (Ross et al. 2012). From the ffERG response, the a-wave amplitude is measured from baseline to trough, the b-wave amplitude from trough to peak and the latency from stimulus onset to the a-wave trough or b-wave peak. Immediately following the ffERG, the jet electrodes are replaced with DTL corneal electrodes and the light adapted mfERG is recorded. The mfERG stimulus is positioned relative to the optic nerve head, using a fundus image that is captured within the FMS VERIS System software (Electrodiagnostic, Inc). The same software controls stimulus presentation. Responses are captured within the visual streak as well as areas temporal, nasal, inferior and superior to it. Responses at each location are positioned relative to the fundus image to align them with the response spatial density profile. Topographic and response amplitude maps are calculated by averaging individual n1-p1 response amplitudes.

Primary cell culture and real time PCR

Primary pig neural retina culture was described previously (Zhou et al. 2011) as was isolation and culture of pig RPE (Liu et al. 2010) and Muller cells (Hicks, and Courtois 1990). RNA isolation and real time PCR was described previously (Zhou et al. 2011). Primers and conditions are described in Table S1. Results were normalized to both actin and GAPDH mRNA levels with similar results.

Analysis of fluorescent-2-deoxy-glucose in vivo

Heterozygous P23H Rho knock in mice (Sakami et al. 2011) or WT litermates were injected with 150 ul of 10 uM fluorescently labeled 2-deoxy-glucose (ThermoFisher Scientific) in the tail vein at P35. Immunofluorescence was analyzed at 15 min, 1 hr and 2 hr timepoints after injection, as described (Rajaram et al. 2013; Frees et al. 2014). At this time, eyes were frozen and sections were analyzed microscopically for fluroescence using optical filters designed for fluorescein. Notably, no fluorescent lableing was seen in mice following sham tail vein injections.

Statistics

Significance was calculated by Student’s t-test. Power was calculated for a one-sample Z-test. Error bars in figures are standard deviations.

Supplementary Material

Refer to Web version on PubMed Central for supplementary material.

Acknowledgments

We thank Connie Cepko and Josh Sanes for valuable constructive comments on the manuscript, Giurong Liu for histologic sectioning and Aaron Rising, Eric Vukmanic, Juan Fernandez de Castro and Paul DeMarco for assistance with ERG measurements. These studies were supported by grants from the NEI, American Health Assistance Foundation, and Research to Prevent Blindness.

References

Adler L, Chen C, Koutalos Y. Mitochondria contribture to NADPH generation in mouse rod photoreceptors. J Biol Chem. 2014; 289:1519–28. [PubMed: 24297174]

Aït-Ali N, Fridlich R, Millet-Puel G, Clérin E, Delalande F, Jaillard C, Blond F, Perrocheau L, Reichman S, Byrne LC, Olivier-Bandini A, Bellalou J, Moyse E, Bouillaud F, Nicol X, Dalkara D, van Dorsselaer A, Sahel JA, Léveillard T. Rod-derived cone viability factor promotes cone survival by stimulating aerobic glycolysis. Cell. 2015; 161:817–32. [PubMed: 25957687]

Anders AM, Ratliff EP, Sachithanantham S, Hui ST. Diminished AMPK signaling response to fasting in thioredoxin-interacting protein knockout mice. FEBS letters. 2011; 585:1223–30. [PubMed: 21439280]

Bainbridge JW, Mehatm MS, Sundaramm V, Robbiem SJ, Barkerm SE, Ripamontim C, Georgiadism A, Mowatm FM, Beattiem SG, Gardnerm PJ, Feathersm KL, Luongm VA, Yzerm S, Balagganm K, Viswanathan A, de Ravel TJ, Casteels I, Holder GE, Tyler N, Fitzke FW, Weleber RG, Nardini M, Moore AT, Thompson DA, Petersen-Jones SM, Michaelides M, van den Born LI, Stockman A, Smith AJ, Rubin G, Ali RR. Long-term effect of gene therapy on Leber's congenital amaurosis. N Engl J Med. 2015; 372:1887–9710. [PubMed: 25938638]

Beltran WA, Cideciyan AV, Iwabe S, Swider M, Kosyk MS, McDaid K, Martynyuk I, Ying GS, Shaffer J, Deng WT, Boye SL, Lewin AS, Hauswirth WW, Jacobson SG, Aguirre GD. Successful arrest of photoreceptor and vision loss expands the therapeutic window of retinal gene therapy to later stages of disease. Proc Natl Acad Sci U S A. 2015 Oct 12. pii: 201509914 Epub ahead of print.

Boye SE, Boye SL, Lewin AS, Hauswirth WW. A comprehensive review of retinal gene therapy. Mol Ther. 2013; 21:509–19. [PubMed: 23358189]

Brown GK, Otero LJ, LeGris M, Brown RM. Pyruvate dehydrogenase deficiency. J Med Genet. 1994; 31:875–79. [PubMed: 7853374]

Bryne LC, Dalkara D, Luna G, Fisher SK, Clérin E, Sahel JA, Léveillard T, Flannery JG. Viral-mediated RdCVF and RdCVFL expression protects cone and rod photoreceptors in retinal degradation. J Clin Invest. 2015; 125:105–116. [PubMed: 25415434]

Burket CT, Montgomery JE, Thummel R, Kassen SC, LaFave MC, Langenau DM, Zon LI, Hyde DR. Generation and characterization of transgenic zebrafish lines using different ubiquitous promoters. Transgenic res. 2008; 17:265–79. [PubMed: 17968670]

Busskamp V, Duebel J, Balya D, Fradot M, Viney TJ, Siegert S, Groner AC, Cabuy E, Foster V, Seeliger M, Biel M, Humphries P, Pagues M, Mohand-Said S, Trono D, Deisseroth K, Sahel JA, Picaud S, Roska B. Genetic reactivation of cone photoreceptors restores visual responses in retinitis pigmentosa. Science. 2010; 329:413–7. [PubMed: 20576849]

Busskamp V, Picaud S, Sahel JA, Roska B. Optogenetic therapy for retinitis pigmentosa. Gene Ther. 2012; 19:169–75. [PubMed: 21993174]

Busskamp V, Krol J, Nelidova D, Daum J, Szikra T, Tsud B, Jüttner J, Farrow K, Scherf BG, Alvarez CP, Genoud C, Sothilingam V, Tanimoto N, Stadler M, Seeliger M, Stoffel M, Filipowicz W, Roska B. mirnas 182 and 183 are necessary to maintain adult cone photoreceptor outer segments and visual function. Neuron. 2014; 83:586–95. [PubMed: 25002228]

Cai CX, Locke KG, Ramachandran R, Birch DG, Hood DC. A comparison of progressive loss of the ellipsoid zone (EZ) band in autosomal dominant and x-linked retinitis pigmentosa. Invest Ophthal Vis Sci. 2014; 55:7417–22. [PubMed: 25342618]

Cerniglia GJ, Dey S, Gallagher-Colombo SM, Daurio NA, Tuttle S, Busch TM, Lin A, Sun R, Esipova TV, Vinogradov SA, Denko N, Kourmenis C, Maity A. The PI3K/AKT pathway regulates oxygen metabolism via pyruvate dehydrogenase (PDH)-E1a phosphorylation. Mol Cancer Ther. 2015; 14:1928–38. [PubMed: 25995437]

Chandler MJ, Smith PJ, Samuelson DA, MacKay EO. Photoreceptor density of the domestic pig retina. Vet Opthalmol. 1999; 2:179–84.

Chen J, Hui ST, Couto FM, Mungrue IN, Davis DB, Attie AD, Lusis AJ, Davis RA, Shalev A. Thioredoxin-interacting protein deficiency induces Akt/Bcl-xl signaling and pancreatic beta-cell mass and protects against diabetes. FASEB J. 2008; 22:3581–94. [PubMed: 18552236]

Chen B, Cepko CL. Requirement of histone deacetylase activity for the expression of critical photoreceptor genes. BMC Dev Biol. 2007; 7:78. [PubMed: 17603891]

Chen B, Cepko CL. HDAC4 regulates neuronal survival in normal and diseased retinas. Science. 2009; 323:256–9. [PubMed: 19131628]

DeBalsi KL, Wong KE, Koves TR, Slentz DH, Seiler SE, Wittmann AH, Ilkayeva OR, Stevens RD, Perry CG, Lark DS, Hui ST, Szweda L, Neufer PD, Muoio DM. Targeted metabolomics connects thioredoxin interacting proteins (txnip) to mitochondrial fuel selection and regulation of specific oxidoreductase enzymes in skeletal muscle. J Biol Chem. 2014; 289:8106–20. [PubMed: 24482226]

El-Azab MF, Baldowshi BR, Mysona BA, Shanab AY, Mohamed IN, Abdelsaid MA, Matragoon S, Bollinger KE, Saul A, El-Remessy AB. Deletion of thioredoxin-interacting protein perserves retinal neuronal function by preventing inflammation and vasuclar injury. Br J Pharmacol. 2014; 171:1299–313. [PubMed: 24283717]

Frees AE, Rajaram N, McCachren SS, Fontanella AN, Dewhirst MW. Delivery-corrected imaging of fluorescently-labeled glucose reveals distinct metabolic phenotypes in murine breast cancer. PLOSone. 2014; 9:e115529.

Geng H, Harvey CT, Pittenbarger J, Liu Q, Beer TM, Xue C, Qian DZ. HDAC4 protein regulates Hif1a protein lysine acetylation and cancer cell response to hypoxia. J Biol Chem. 2011; 286:38095–102. [PubMed: 21917920]

Gospe SM, Sheila A, Baker SA, Vadim Y, Arshavsky VY. Facilitative glucose transporter Glut1 is actively excluded from rod outer segments. J cell Sci. 2010; 123:3639–3644. [PubMed: 20923839]

Hendrickson A, Hicks D. Distribution and density of medium- and short-wavelength selective cones in the domestic pig retina. Exp Eye Res. 2002; 74:435–44. [PubMed: 12076087]

Hui ST, Andres AM, Miller AK, Spann NJ, Potter NM, Chen AZ, Sachithanantham S, Jung DY, Kim JK, Davis RA. Txnip balances metabolic and growth signaling via PTEN disulfide reduction. Proc Natl Acad Sci USA. 2008; 105:3921–6. [PubMed: 18322014]

Hicks D, Courtois Y. The growth and behavior of rat retinal Müller cells in vitro. 1. An improved method for isolation and culture. Exp Eye Res. 1990; 51:119–29. [PubMed: 2387332]

Hurley JB, Lindsay KJ, Du J. Glucose, lactate, and shuttling of metabolites in vertebrate retinas. J Neurosci Res. 2015; 93:1079–92. [PubMed: 25801286]

Jacobson SG, Cideciyan AV, Roman AJ, Sumaroka A, Schwartz SB, Heon E, Hauswirth WW. Improvement and decline in vision with gene therapy in childhood blindness. N Engl J Med. 2015; 372:1920–6. [PubMed: 25936984]

Jeon TI, Esquejo RM, Roqueta-Rivera M, Phelan PE, Moon YA, Govindarajan SS, Esau CC, Osborne TF. An srebp responsive micro-rna operon contributes to a regulatory loop for intracellular lipid hemeostasis. Cell Metab. 2013; 18:51–61. [PubMed: 23823476]

Kwon J, Lee SR, Yang KS, Ahn Y, Kim YJ, Stadtman ER, Rhee SG. Revesible oxidation and inactivation of the tumor suppressor pten in cells stimulated with peptide growth factors. Proc Natl Acad Sci USA. 2004; 101:16419–24. [PubMed: 15534200]

Lin B, Masland RH, Stettoi E. Remodeling of cone photoreceptors after rod degeneration in rd mice. Exp Eye Res. 2009; 88:589–99. [PubMed: 19087876]

Liu Y, Xin Y, Fei Y, Wang W, Lu Q, Kaplan HJ, Dean DC. Taz-Tead1 Links Cell-Cell Contact to Zeb1 Expression, Proliferation and Dedifferentiation in Retinal Pigment Epithelial Cells. Invest Ophthal Vis Sci. 2010; 51:3372–8. [PubMed: 20207963]

Liu Y, Sánchez-Tilló E, Lu X, Clem B, Telang S, Jenson AB, Cuatrecasas M, Chesney J, Postigo A, Dean DC. Rb1 family mutation is sufficient for sarcoma initiation. Nat Commun. 2013; 4:2650. [PubMed: 24150016]

Liu Y, Sánchez-Tilló E, Lu X, Huang L, Clem B, Telang S, Jenson AB, Cuatrecasas M, Chesney J, Postigo A, Dean DC. The ZEB1 transcription factor acts in a negative feedback loop with miR200 downstream of Ras and Rb1 to regulate Bmi1 expression. J Biol Chem. 2014; 289:4116–25. [PubMed: 24371144]

Litts KM, Messinger JD, Freund KB, Zhang Y, Curcio CA. Inner segment remodeling and mitochondrial translocation in cone photoreceptors in age-related macular degeneration with outer retinal tubulation. Retina. 2015; 56:2243–53.

Lumayag S, Haldin CE, Corbett NJ, Wahlin KJ, Cowan C, Turturro S, Larsen PE, Kovacs B, Witmer PD, Valle D, Zack DJ, Nicholson DA, Xu S. Inactivation of the microrna-183/96/182 cluster results in syndromic retinal degeneration. Proc Natl Acad Sci USA. 2013; 110:507–16. [PubMed: 23267087]

Marin-Hernandez A, Gallardo-Perez JC, Ralph SJ, Rodriquez-Enriquez S, Moreno-Sanchez R. Hif1alpha modulates energy metabolism in cancer cells by inducing over-expression of specific glycolytic isoforms. Mini Rev Med Chem. 2009; 9:1084–101. [PubMed: 19689405]

Morrow EM, Furukawa T, Cepko CL. Vertebrate photoreceptor cell development and disease. Trends Cell Biol. 1998; 8:353–357. [PubMed: 9728396]

Mussolino C, della Corte M, Rossi S, Viola S, Di Vicino U, Marrocco E, Neglia S, Doria M, Testa F, Giovannoni R, Crasta M, Giunti M, Villani E, Lavitrano M, Bacci ML, Ratigila R, Simonelli F, Auricchio A, Surace EM. AAV-mediated photoreceptor transduction of the pig cone-enriched retina. Gene Therapy. 2011; 18:637–45. [PubMed: 21412286]

Patwari P, Lee RT. An expanded family of arrestins regulate metabolism. Trends Endocrinol Metab. 2012; 23:216–22. [PubMed: 22520962]

Penha FM, Maia M, Eid Farah M, Príncipe AH, Freymüller EH, Maia A, Magalhães O Jr, Smith RL. Effects of subretinal injections of indocyanine green, trypan blue and glucose in rabbit eyes. Ophthalmology. 2007; 114:899–908. [PubMed: 17292475]

Price BA, Sandoval IM, Chan F, Simons DL, Wu SM, Wensel TG, Wilson JH. Mislocalization and degradation of human P23H-rhodopsin-GFP in a knockin mouse model of retinitis pigmentosa. Invest Ophthalmol Vis Sci. 2011; 52:9728–36. [PubMed: 22110080]

Rajaram N, Frees AE, Fontanella AN, Zhong J, Hansen K, Dewhirst MW. Delivery rate affects uptake of a fluorescent glucose analog in murine metastatic breast cancer. PLOSone. 2013; 8:e76524.

Roof DJ, Adamian M, Hayes A. Rhodopsin accumulation at abnormal sites in retinas of mice with a human P23H rhodopsin transgene. Invest Ophthalmol Vis Sci. 1994; 35:4049–62. [PubMed: 7960587]

Ross JW, Fernandez de Castro JP, Zhao J, Samuel M, Walters E, Rios C, Bray-Ward P, Jones BW, Marc RE, Wang W, Zhou L, Noel JM, McCall MA, DeMarco PJ, Prather RS, Kaplan HJ. Generation of an inbred pig model of retinitis pigmentosa. Invest Ophthalmol Vis Sci. 2012; 53:501–507. [PubMed: 22247487]

Sahel JA, Roska B. Gene therapy for blindness. Annu Rev Neurosci. 2013; 36:467–88. [PubMed: 23724995]

Sahel JA, Leveillard T, Picaud S, Dalkara D, Marazova K, Safran A, Paques M, Duebel J, Roska B, Mohand-Said S. Functional rescue of cone photoreceptors in retinitis pigmentosa. Grafes Arch Clin Exp Ophthalmol. 2013; 251:1669–77.

Sakami S, Maeda T, Bereta G, Okano K, Golczak M, Sumaroka A, Roman AJ, Cideciyan AV, Jacobson SG, Palczewski K. Probing mechanisms of photoreceptor degeneration in a new mouse model of the common form of autosomal dominant retinitis pigmentosa due to P23H opsin mutations. J Biol Chem. 2011; 286:10551–67. [PubMed: 21224384]

Saliba RS, Munro PM, Luthert PJ, Cheetham ME. The cellular fate of mutant rhodopsin: quality control, degradation and aggresome formation. J Cell Sci. 2002; 115:2907–18. [PubMed: 12082151]

Scott PA, Fernandez de Castro JP, Kaplan HJ, McCall MA. A pro23his mutation alters prenatal rod photoreceptor morphology in a transgenic swine model of retinitis pigmentosa. Retina. 2014; 55:2452–59.

Tam BM, Qazalbash A, Lee HC, Moritz OL. The dependence of retinal degeneration caused by the rhodopsin P23H mutation on light exposure and vitamin a deprivation. Invest Ophthalmol Vis Sci. 2010; 51:1327–34. [PubMed: 19933196]

Taylor MR, Hurley JB, Van Epps HA, Brockerhoff SE. A zebrafish model for pyruvate dehydrogenase deficiency: rescue of a neurological dysfunction and embryonic lethality using a ketogenic diet. Proc Natl Acad Sci USA. 2004; 101:4584–9. [PubMed: 15070761]

Van Soest S, Westerveld A, de Jong PT, Bleeker-Wagemakers EM, Bergen AA. Retinitis pigmentosa: defined from a molecular point of view. Survey Ophthamol. 1999; 43:321–334.

Wang W, Fernandez de Castro J, Vukmanic E, Zhou L, Emery D, Demarco PJ, Kaplan HJ, Dean DC. Selective rod degeneration and partial cone inactivation characterize an iodoacetic acid model of swine retinal degeneration. Invest Ophthalmol Vis Sci. 2011; 52:7917–23. [PubMed: 21896868]

Wang W, Zhou L, Lee SJ, Liu Y, Fernandez de Castro J, Emery D, Vukmanic E, Kaplan HJ, Dean DC. Swine cone and rod precursors arise sequentially and display sequential and transient integration and differentiation potential following transplantation. Invest Ophthalmol Vis Sci. 2014; 55:301–9. [PubMed: 24327609]

Warburg O. Science. On respiratory impairment in cancer cells. Science. 1956; 124:269–70. [PubMed: 13351639]

Williams RW. The human retina has a cone-rich rim. Visual Neurosciences. 1991; 6:403–6.

Wong F, Kwok SY. The survival of cone photoreceptors in retinitis pigmentosa. JAMA Ophthalmol. 2016 Published online January 7, 2016.

Xu G, Chen J, Jing G, Shalev A. Thioredoxin-interacting protein regulates insulin transcription through microRNA-204. Nat Med. 2013; 19:3287–94.

Xu X, So JS, Park JG, Lee AH. Transcriptional control of hepatic metabolism by srebp and chrebp. Semin Liver Dis. 2013; 33:301–11. [PubMed: 24222088]

Yoshioka J, Chutkow WA, Lee S, Kim JB, Yan J, Tian R, Lindsey ML, Feener EP, Seidman CE, Seidman JG, Lee RT. Deletion of thioredoxin-interacting protein in mice impairs mitochondrial function but protects the myocardium from ischemia-reperfusion injury. J Clin Invest. 2012; 122:267–279. [PubMed: 22201682]

Zhen C, Baum BJ. All human EF1a promoters are not euqal: markedly affect gene expression in constructs from different sources. Int J Med Sci. 2014; 11:404–8. [PubMed: 24688302]

Zhou L, Wang W, Liu Y, Fernandez de Castro J, Ezashi T, Telugu BP, Roberts RM, Kaplan HJ, Dean DC. Differentiation of induced pluripotent stem cells of swine into rod photoreceptors and their integration into the retina. Stem Cells. 2011; 29:972–80. [PubMed: 21491544]

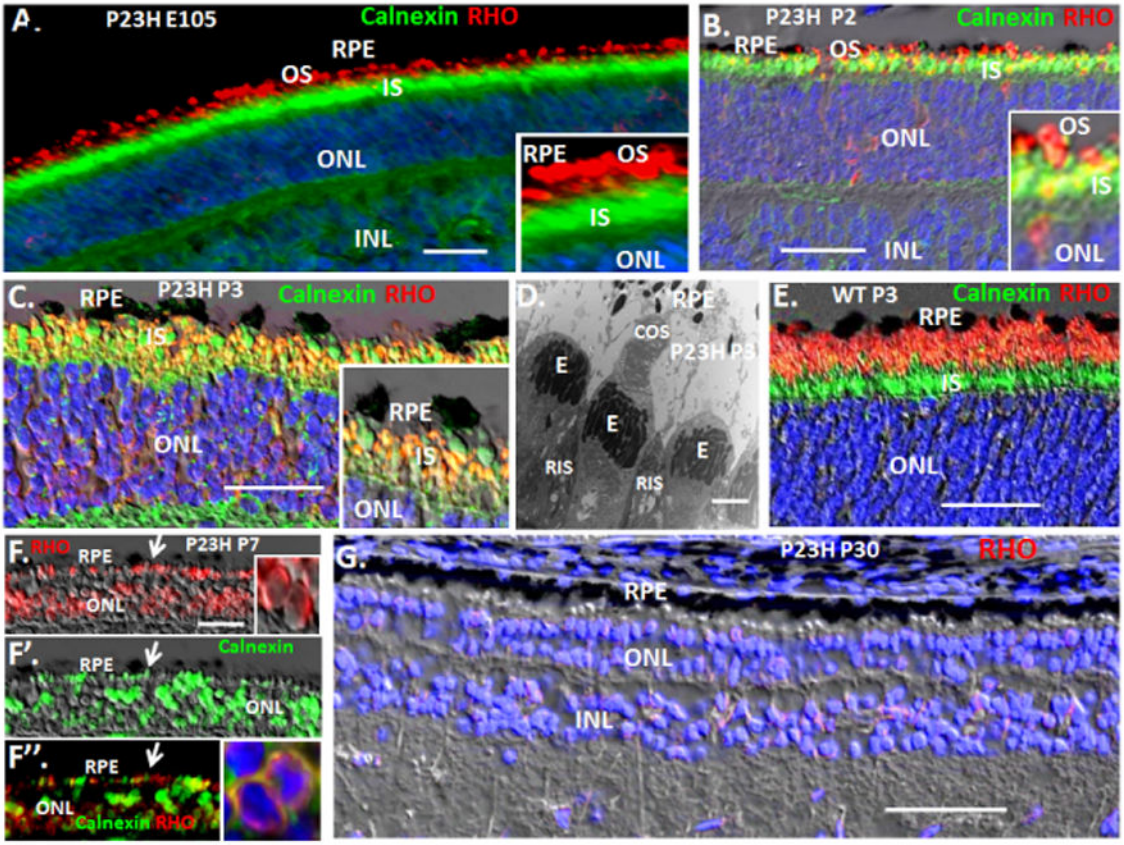

Fig. 1. RHO$^+$ OS form initially in WT and P23H embryonic retinas, but P23H RHO becomes sequestered in inner segments (IS) shortly after birth where it aggregates with WT RHO to cause its dominant retention in IS, thereby causing loss of rod OS

(A) Immunostaining of a P23H retinal section at E105 (gestation in the pig is ~113 days) showing RHO$^+$ OS. Calnexin is an ER marker that denotes IS. (B) By P2 in the P23H retina, RHO is becoming trapped in calnexin$^+$ rod IS. (C) Both mutant and WT RHO are sequestered in many calnexin$^+$ rod IS at P3 in P23H retinas. (D) EM, showing loss of rod OS and onset of cone OS loss at P3 in P23H retinas. "E" cone ellipsoid, containing mitochondria. (E) RHO$^+$ OS persist and extend after birth in WT retinas. (F) By P7, P23H rod IS collapse to a perinuclear calnexin$^+$, RHO$^+$ structure. (G) RHO$^+$ rods are lost in the P23H retina by P30. RIS, rod IS; CIS, cone IS. Blue is Dapi. Bars are 2 μm in the EM in panel D, and 30 μm in other panels. See Fig. S1 for quantification of rod OS and rod cell loss and for quantification of cone OS loss.

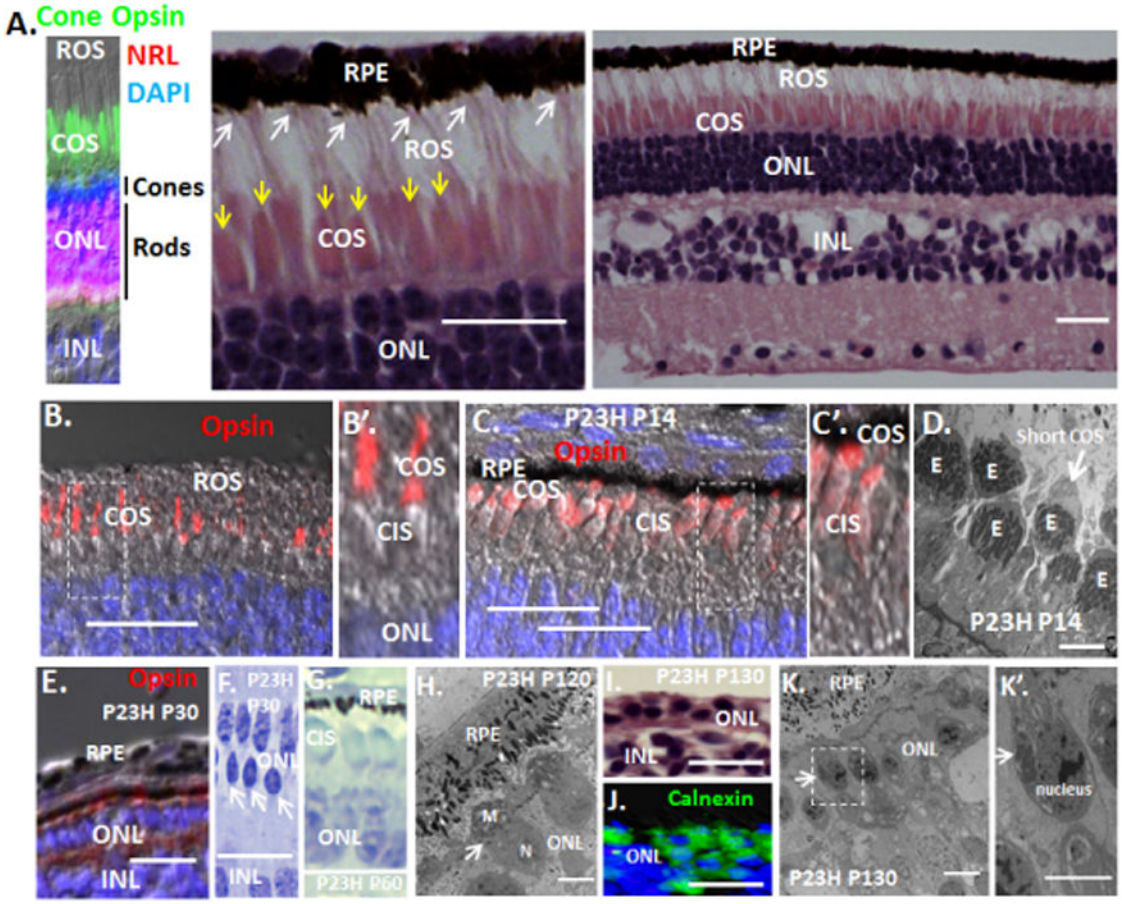

Fig. 2. Loss of cone OS synthesis initiates with rod OS loss in P23H pigs following birth, and then four months later IS disassemble

(A) Interaction of long rod OS (white arrows) with the RPE in WT P14 pig retina. Shorter cone OS are shown by yellow arrows. Note, cones are confined to the two outer rows of the ONL, whereas NRL^+ rods are limited to the inner ONL rows in pigs. (B and B′). Long cone OS in the WT P14 pig retina. The box indicates the region of higher magnification in B′. (C and C′) By P14, P23H have diminished OS synthesis and persisting OS are shortened (See Fig. S1 for quantification). The box indicates the region of higher magnification in C′. (D) EM showing diminished cone OS in P23H pigs at P14. “E” cone ellipsiod, containing mitochondria. (E) Cones continue to lose $opsin^+$ OS at P30. See Fig. S1 for quantification. (F) The ONL at P30 consists primarily of cones, and persisting rods (arrows) show compacted dense nuclei. (G) By P60, the P23H ONL is comprised only of cones (noted by their distinctive nuclear ellipsoid shape and chromatin staining pattern), which lack OS but maintain IS. (H) At P120, cone IS are compressed and the cilium (arrow) is lost. “N” cone nucleus; “M” mitochondria. (I) H&E section showing loss of both OS and IS in the 1–2 rows of dormant cones persisting at P130. (J) Immunostaining for the ER marker calnexin demonstrates ER collapse into the cell body at P130. (K and K′) EM showing migration of mitochondria from the IS to perinuclear postions (arrows) at P130. The bar in the EM is 2 μm, other bars are 30 μm.

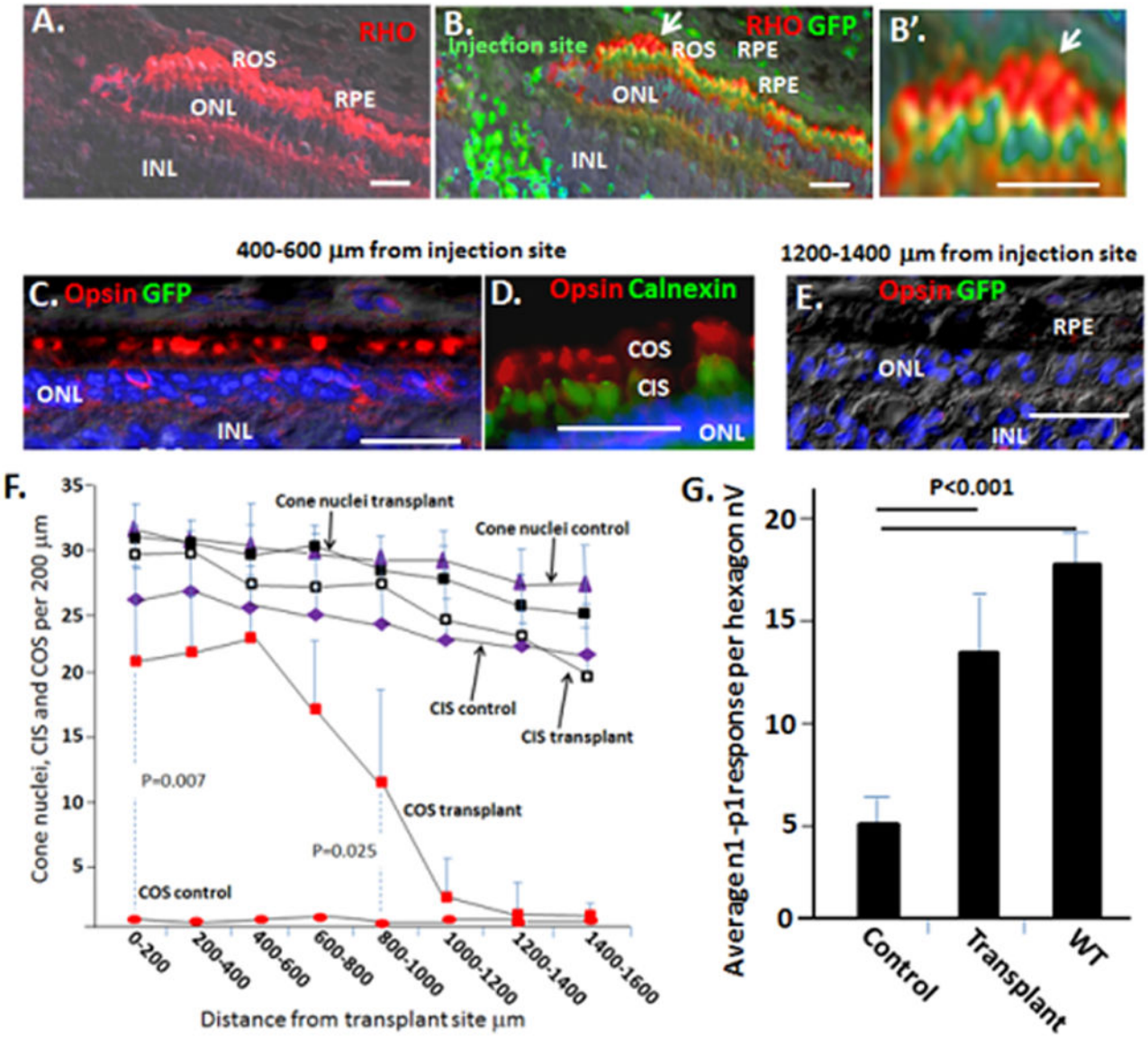

Fig. 3. Transplantation of WT GFP$^+$ rod precursors into the subretinal space of P23H pigs preserves endogenous cone OS and electrophysiology

(A and B) Rod precursors were transplanted in the region of the visual streak in P23H pigs at P14, and assessment was at P60. Representative immunostaining is shown. Note GFP$^+$ transplanted rod precursors integrate into the ONL and form long RHO$^+$ OS at the injection site. The arrow in panel B shows the region of higher magnification in panel B′. (C–E) Endogenous COS (GFP$^-$) in transplant recipients, but not controls, are maintained at a distance of 400–600 µm but not 1200–1400 µm from the injection site. Calnexin marks the ER in IS. Also, see Fig. S2–S4. (F) Quantification of cone number, cone IS and cone OS following rod precursor transplant. Although P23H pigs at P60 lack cone OS, based on cone OS number and standard deviation in WT pigs (see Fig. 4H and 6K below), we calculated that 4 samples would be required to observe a 50% change in cone OS number with a power of 0.95. Cone histology was then analyzed in four vectors (inferior, superior, temporal and

nasal) from each transplant site. n=5. Also, see Fig. S4. Vectors from the transplant sites were then averaged. Error bars are standard deviations. Note, sham transplants in the contralateral eyes had no significant effect on COS. (G) Transplantation of GFP^+ rod precursors into the subretinal space of P23H pigs preserves mfERG. Initial trough-to-peak amplitudes of b wave signals (n1-p1) in hexagons surrounding injection sites were averaged. See Figs. S2 for representative mfERGs and areas used for quantification. Error bars are standard deviations. Bars are 30 μm.

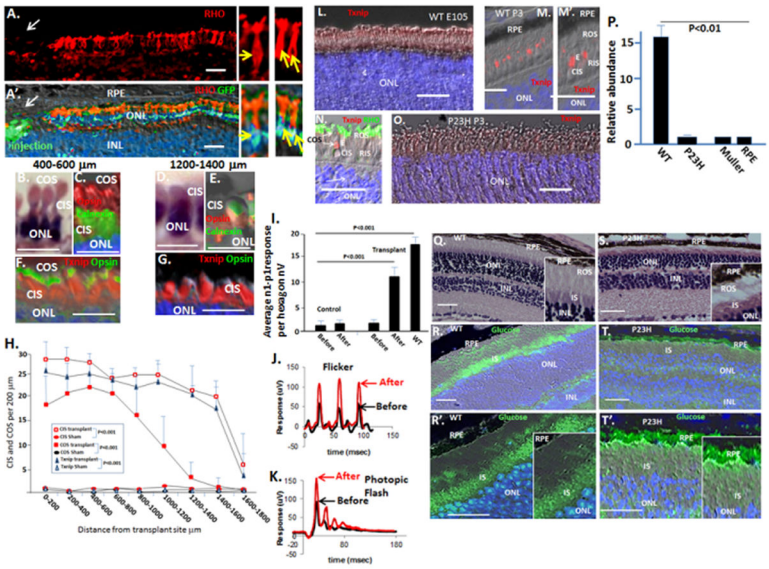

Fig. 4. Glucose becomes sequestered in the RPE and is not transported to photoreceptors in the P23H retina. Transplant of GFP$^+$ rod precursors restores cone access to glucose, and reverses end-stage cone dormancy restoring cone inner (CIS), cone outer sgements (COS) and electrophysiology in the P23H retina

(A and A′) 5 × 10^5 E65 rod precursors were transplanted subretinally at two separate sites in the visual streak of 18 month old P23H pigs, as in Fig. 3, and assessment was done 5 weeks later. Immunostaining shows the GFP$^+$ transplanted cells formed a monolayer, extending long RHO$^+$ OS to the RPE at sites of injection. Yellow arrows indicate GFP$^+$ nuclei in transplanted cells extending RHO$^+$ OS in the higher power images on the right. Also, see Fig. S2–3. n=4. (B) H&E section showing restoration of endogenous CIS and COS in the region 400–600 µm from the injection site. (C) Calnexin staining highlights CIS, and cone opsin staining shows OS in this region. (D and E) Calnexin+ cone IS are maintained out to 1400 µm from the cell injection site, whereas OS restoration is lost at this distance. (F and G) Txnip induction marks restored CIS out to 1400 µm, although cone OS were only restored to 1000 µm. (H) Quantification of CIS, COS and Txnip expression was evaluated in multiple vectors from injection sites, as noted above (see Fig. S4). Error bars are standard deviations. (I) mfERG is increased in region surrounding cell transplants. Quantification of mfERG signals in hexagons surrounding transplant sites is shown, as in Fig. 3. Error bars are standard deviations. Sites of cell transplant in the optic cup and representative mfERGs are shown in Fig. S3. (J and K) Representative photopic ffERGs (photopic flash and flicker) are shown before and after cell transplant. (L–O) Immunostaining showing Txnip is induced in the distal end of WT CIS (the ellipsoid where mitochondria are concentrated) following birth, but it is not induced in the P23H retina. (P) Real time PCR showing relatively low levels of Txnip mRNA in P23H neural retina at P14, and in primary cultures of RPE and Muller cells (also see Fig. S6). (Q–T′) Fluorescent 2-deoxy-glucose was injected in the tail vein of P23H Rho knock in mice (S–T′) (n=4) and WT litermates (Q–R′) (n=4) at P35, and frozen eye sections were analyzed 1 hr later. Bars are 30 µm.

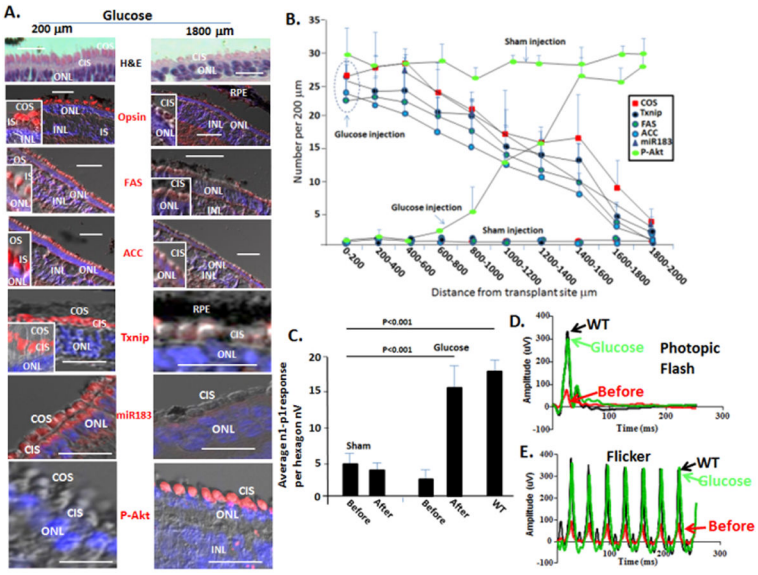

Fig. 5. Subretinal glucose injection rapidly reactivates cone OS synthesis, induces Txnip, fatty acid synthesis enzymes and miR-183, and restores photopic ffERG to a WT level in P23H retinas

(A) Glucose was injected at P45, and eyes were examined 3 days after injection. Sham indicates injection of control media into the contralateral eye. Bars are 40 µm. Representative H&E, immunostaining and in situ hybridization after glucose injection showing that OS are restored and Txnip, FAS, ACC and miR-183 are induced in endogenous cones in the region of the injection site. (B) Quantification of immunostaining and in situ hybridization in panel A, as described in Figs. 3–4 and S4 and 5. n=4. Error bars are standard deviations. $p<0.01$ for all comparisons between glucose and sham injection. (C) Subretinal glucose injection restores mfERG. Quantification of mfERG signals in hexagons surrounding injection sites is shown. Representative mfERGs are shown in Fig. S5. Error bars are standard deviations. (D and E) Representative photopic ffERG (photopic flash and flicker) before and after glucose injection. WT litermate ffERGs are shown for comparison. As with mfERG in panel B, sham injection did not increase the ffERG.

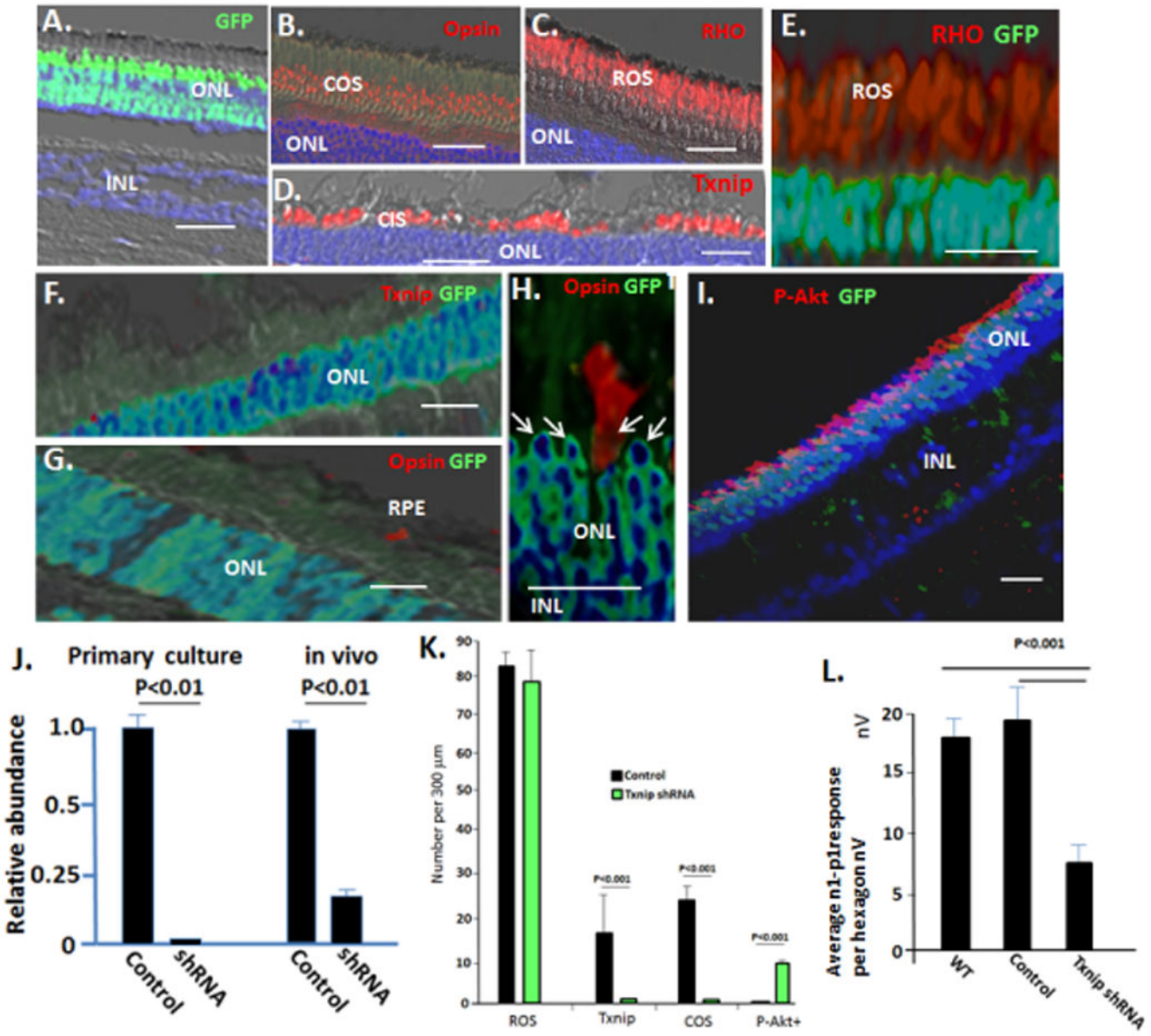

Fig. 6. Subretinal injection of AAV expressing Txnip shRNAs inhibits cone OS synthesis and electrophysiology and induces constitutive activation of Akt in cones, but it does not affect rod OS formation or rod electrophysiology

AAV viruses (Fig. S6) were injected in 30 µl subretinally into the region of the visual streak in WT pigs at P60, as described for cells and glucose in Figs. 3–5. Eyes were harvested after 4 weeks. (A–D) Control AAV expressing GFP and a scrambled Txnip shRNA sequence (Fig. S6) infects photoreceptors, but does not affect expression of Txnip or formation of cone or rod OS. (E) AAV expressing Txnip shRNA and GFP does not affect RHO^{+} rod OS formation or electrophysiology (Fig. S6). (F) Txnip shRNA AAV inhibits Txnip expression. (G–H) AAV expressing Txnip shRNA inhibits cone $opsin^{+}$ OS formation. Note $opsin^{+}$ cone OS are confined to uninfected GFP^{-} cells. Arrows indicate cone nuclei, which are confined to the outer two rows of the ONL, where rods are excluded (Fig. 2A). (I) AAV expressing

Txnip shRNA causes activation of Akt (P-Akt) in cones, which as noted, comprise the outer two ONL rows in the pig. Note infected rods, which make up the inner rows of the ONL, do not activate Akt. GFP is not expressed from the viral EF1a promoter following infection of RPE or Muller cells (Fig. S6). (J) Real time PCR analyzing expression of Txnip mRNA in WT neural retina following infection with AAV Txnip shRNA in vivo (as in panels A–I, see Fig. S6 for viral GFP expression in the optic cup and sites of RNA isolation), and in vitro in primary culture of WT neural retina at P14. (K) Quantification of results in panels A–I. (L) Quantification of the effects of AAV on photopic mfERG. See Fig. S6 for representative mfERG and ffERGs. Control virus n=5; Txnip shRNA viruses n=8. Bars are 30 μm. Standard deviations are shown.

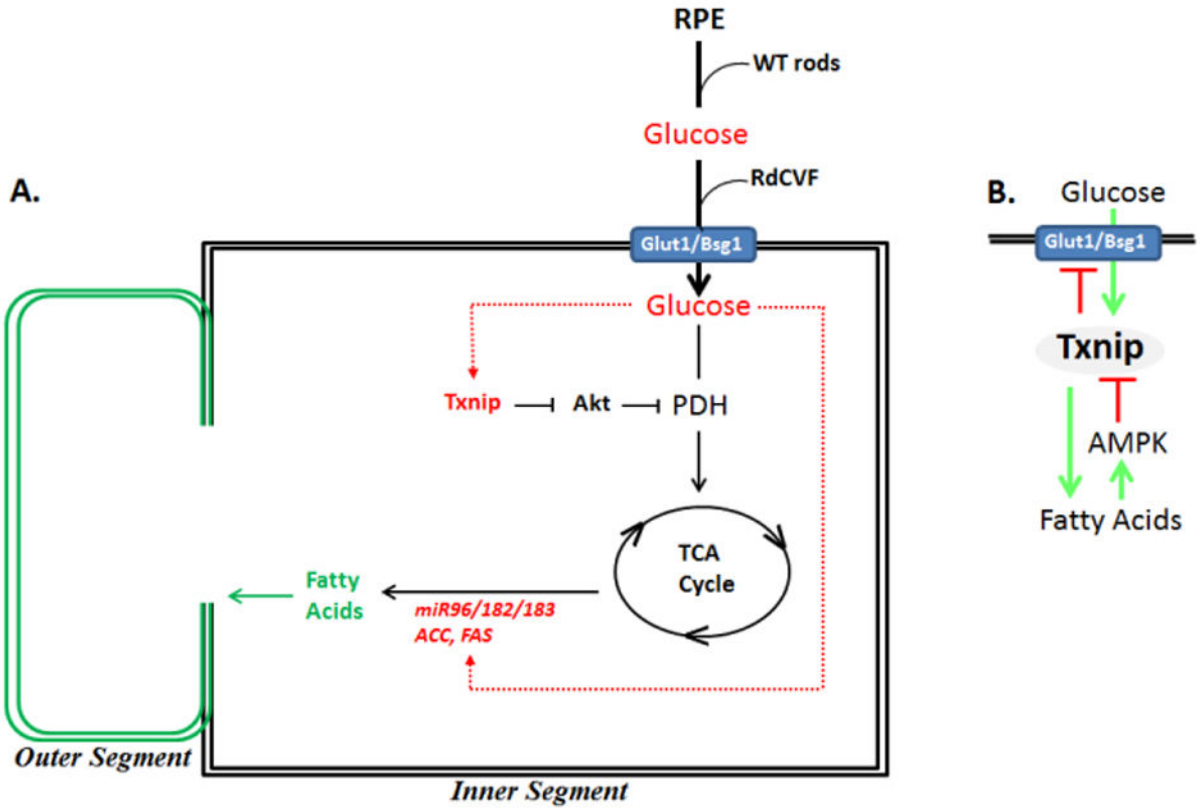

Fig. 7. Transplant of rod precursors restores acces of cones to glucose in the P23H retina where glucose in turn regulates its own metabolic pathway

(A) Proposed pathways in rod-mediated reactivation of end-stage dormant cones in RP. (B) Txnip as a regulator of glucose metabolism to fatty acids. See text for discussion.